Neutron diffraction refinement and characterization of $FeRGe_2O_7$ (R = La, Pr, Nd, Gd)

1996 J. Phys.: Condens. Matter 8 2641

(http://iopscience.iop.org/0953-8984/8/15/013)

J. Phys.: Condens. Matter **8** (1996) 2641–2653. Printed in the UK

Neutron diffraction refinement and characterization of $FeRGe_2O_7$ (R = La, Pr, Nd, Gd)

L Bucio†, C Cascales, J A Alonso and I Rasines

Instituto de Ciencia de Materiales de Madrid, CSIC, Cantoblanco, E-28049 Madrid, Spain

Received 24 October 1995, in final form 23 January 1996

Abstract. From stoichiometric mixtures of analytical grade Fe_3O_4, R_2O_3 or Pr_6O_{11} and GeO_2, polycrystalline samples of four iron rare-earth germanates $FeRGe_2O_7$ (R = La, Pr, Nd, Gd) have been prepared. They are monoclinic, S.G. $P2_1/c$ (No 14) and $Z = 4$, isotypic with $AlRGe_2O_7$. Results of the refinements from neutron (R = La, Pr) powder diffraction data by the Rietveld method of profile analysis as well as x-ray (R = Nd, Gd) powder diffraction data are given. The four x-ray diffraction powder patterns are included together with lattice dimensions, which decrease from a (Å) = 7.308(1), b (Å) = 6.667(1), c (Å) = 13.065(2), β (°) = 117.18(1) and V (Å^3) = 566.3(1) for R = La to a (Å) = 7.141(1), b (Å) = 6.5903(7), c (Å) = 12.833(2), β(°) = 117.08(2) and V (Å^3) = 537.73(9) for R = Gd. Magnetic susceptibility measurements between 350 and 1.7 K confirm the existence of antiferro-magnetic ordering and Néel temperatures of 4.3, 3.7 and 5.8 K for R = Pr, Nd and Gd, respectively. IR spectra up to 100 cm^{-1} are included and briefly discussed.

1. Introduction

The interesting physical properties and possible applications of the compounds combining 3d transition metals, T, and rare earths, R (either binary intermetallics T–R, or species such as T–R borides, carbides, nitrides and oxides among others) have contributed to increasing efforts in the precise refinement or in some cases the determination of novel crystal structures of this kind of compound. In this way, the possibility of activating single-centred compounds such as cubic garnets or orthorhombic aluminates, of space groups $Ia3d$ and $Pnma$ respectively, with rare-earth or transition-metal cations, suggests the possibility of obtaining self-activated crystals, in which a good number of interesting effects [1] could be found.

The present authors are involved in preparing and studying especially single crystals of compounds with T and R cations embedded in a matrix of p elements, B–O or Ge–O [2–4]. Among germanates of $MRGe_2O_7$ composition only those with M = Al and Ga [5, 1], which present a monoclinic structure type, S.G. $P2_1/c$, are well characterized. The phase formation in polycrystalline samples of the $FeRGe_2O_7$ family has been found [6] to be dependent on the size of R, with two different structures, one for the larger (La–Gd) and the other for the smaller (Tb–Yb and Y) rare-earth ions. Although magnetic studies [7] have been carried out for the larger lanthanide compounds, which display the above-mentioned monoclinic structure, their crystal structure data are not currently available. The present

† Permanent address: Departamento de Estado Sólido, Instituto de Física, UNAM, Apdo. postal 20-364, 01000 Mexico DF Mexico.

0953-8984/96/152641+13$19.50

paper reports the structural characterization of the four title compounds, two of which have been refined by a Rietveld profile analysis from neutron powder diffraction (NPD) data. The results of magnetic susceptibility measurements and IR spectra are also reported.

2. Experimental details

2.1. Preparation of samples

$FeRGe_2O_7$ (R = La, Pr, Nd, Gd) were prepared as polycrystalline powders from stoichiometric mixtures of analytical grade Fe_3O_4, GeO_2 and R_2O_3 or Pr_6O_{11}. Thermal treatments were carried out in air for 5 d from 900 to 1100 °C with intermediate regrindings. The standard x-ray powder diffraction analysis showed final samples as very well crystallized and pure materials.

2.2. Crystallographic analysis

The x-ray powder diffraction patterns for the d-spacing measurements were made using a Siemens Kristalloflex 810 generator, Cu Kα radiation ($\lambda = 1.540\,598$ Å) and a computer-controlled D-500 goniometer equipped with a graphite monochromator. The data were collected at room temperature and a scanning rate of $0.1^\circ\ 2\theta$ min^{-1}, using tungsten, $a = 3.165\,24(4)$ Å, as an internal standard.

The unit cell dimensions were refined from the 2θ values up to 100° 2θ of the more intense, non-axial and individual non-overlapping observed reflections by means of a least-squares refinement program [8].

The NPD diagrams of $FeLaGe_2O_7$ and $FePrGe_2O_7$ were collected at room temperature in the DN5 multidetector diffractometer at the Siloé reactor of the Centre d'Etudes Nucléaires, Grenoble. A wavelength of 1.344 Å was selected from a Cu monochromator. The 800 detectors covered a 2θ range of 80° from $2\theta_i = 10^\circ$. The counting time was about 4 h, using about 6 g of the specimen. The neutron diffraction patterns were analysed by the Rietveld [9] method, using a strongly modified version [10] of the Young and Wiles refinement program [11]. A pseudo-Voigt function was chosen to generate the line shape of the diffraction peaks. The coherent scattering lengths for La, Pr, Fe, Ge and O were, respectively, 8.24, 4.45, 9.54, 8.193 and 5.805 fm. No regions were excluded in the refinements. In the final run the following parameters were refined in the S.G. $P2_1/c$ (No 14): background coefficients, zero-point, half-width, pseudo-Voigt and asymmetry parameters for the peak shape; scale factors, positional, thermal isotropic factors (anisotropic for Pr and constrained for the seven oxygen atoms in $FeLaGe_2O_7$) and unit-cell dimensions. In each case the starting values for the positional parameters used in the refinements were those reported for the isotypic $GaGdGeO_7$ compound [1]. A total number of 53 and 65 independent parameters were refined for the La and Pr germanates, respectively.

On the basis of the structural parameters derived from the neutron data, the XRD patterns were calculated for the four germanates using the program LAZY-PULVERIX [12] and the peaks were carefully indexed in the observed diagrams. The unit-cell parameters were precisely recalculated by least-squares refinement from the observed positions of the reflections, once corrected with respect to tungsten as internal standard.

2.3. Magnetic measurements

A SQUID magnetometer operating from 300 to 1.7 K at 1000 Oe was used to perform the dc magnetic measurements. Between 10 and 1.7 K, magnetization measurements were also carried out in magnetic fields ranging from 1 to 50 kOe. Diamagnetic corrections [13] for magnetic susceptibilities were introduced.

2.4. IR spectra

An FT IR Nicolet SX60 spectrometer was used in the range 4000–100 cm^{-1} with the powdered samples dispersed either in KBr or in polyethylene pellets.

2.5. Results and discussion

The four title compounds were obtained as monophased powders, ochre in colour, with a good crystallinity, although the La-containing material was observed to degrade when stored in air over a period of some weeks. All XRPD patterns obtained are similar to that of the analogue $GaGdGe_2O_7$ [1]. The observed and calculated d-spacings and the observed intensities for each peak, which may consist of several overlapped, not resolved, reflections, have been recorded.

Table 1. Refined atomic coordinates and isotropic thermal parameters for $FeRGe_2O_7$, R = La and Pr. Average esds are in parentheses.

Atom	x	y	z	B_{eq}
La	0.7599(19)	0.1477(19)	0.0189(9)	0.97(25)
Fe	0.7913(14)	0.4014(17)	0.2682(8)	0.52(18)
Ge1	0.7863(19)	0.6544(16)	0.0419(9)	0.62(17)
Ge2	0.2919(18)	0.4050(17)	0.2155(11)	0.62(17)
O(1)	0.5873(26)	0.8130(26)	0.0120(13)	0.52(12)
O(2)	0.7788(23)	0.1064(22)	0.2181(14)	0.52(12)
O(3)	0.5543(21)	0.3649(24)	0.2995(13)	0.52(12)
O(4)	0.0038(25)	0.3284(26)	0.4160(14)	0.52(12)
O(5)	0.7518(27)	−0.0083(19)	0.4221(16)	0.52(12)
O(6)	0.8098(25)	0.4652(24)	0.1316(15)	0.52(12)
O(7)	0.1584(23)	0.1749(25)	0.1882(15)	0.52(12)
Pr	0.7608(22)	0.1468(16)	0.0239(10)	1.43(24)[a]
Fe	0.7891(8)	0.4008(8)	0.2668(5)	0.87(11)
Ge1	0.7857(10)	0.6551(8)	0.0404(5)	0.49(12)
Ge2	0.2924(11)	0.4993(8)	0.2171(6)	0.99(14)
O(1)	0.5885(15)	0.8172(15)	0.0147(8)	1.12(22)
O(2)	0.7831(13)	0.1078(11)	0.2193(7)	0.29(15)
O(3)	0.5633(12)	0.3779(14)	0.3042(7)	1.33(19)
O(4)	0.0062(13)	0.3322(14)	0.4208(7)	0.53(20)
O(5)	0.7480(16)	−0.0074(10)	0.4202(9)	0.78(19)
O(6)	0.7992(15)	0.4553(13)	0.1272(8)	0.89(23)
O(7)	0.1527(14)	0.1863(13)	0.1880(9)	0.89(19)

[a] Anisotropic thermal parameters $\times 10^4$, B_{11} = 165(41), B_{22} = 1.2(30), B_{33} = 22(6), $B_{12} = -23(30)$, $B_{13} = 11(20)$, $B_{23} = 8(18)$.

In spite of the complexity of the structure, containing 14 independent atoms at general positions in the asymmetric unit, the NPD Rietveld refinements on the La and Pr samples

Table 2. Main interatomic distances (Å) and angles (°) in $FeRGe_2O_7$, R = La and Pr. Average esds are in parentheses.

	La	Pr
R–O(1)	2.550(22)	2.494(16)
R–O(1′)	2.403(25)	2.356(21)
R–O(2)	2.549(20)	2.482(15)
R–O(3)	2.560(18)	2.548(14)
R–O(4)	2.618(22)	2.572(16)
R–O(4′)	2.684(24)	2.672(19)
R–O(5)	2.706(18)	2.727(14)
R–O(6)	2.503(20)	2.393(14)
R–O(7)	2.745(22)	2.674(18)
Fe–O(2)	2.058(19)	2.034(9)
Fe–O(3)	1.969(21)	1.913(12)
Fe–O(4)	1.903(20)	1.952(10)
Fe–O(6)	1.895(21)	1.882(12)
Fe–O(7)	1.902(20)	1.971(10)
Ge(1)–O(1)	1.683(23)	1.695(13)
Ge(1)–O(4)	1.804(23)	1.793(12)
Ge(1)–O(5)	1.766(20)	1.756(11)
Ge(1)–O(6)	1.676(20)	1.714(11)
Ge(2)–O(2)	1.800(21)	1.769(11)
Ge(2)–O(3)	1.746(22)	1.774(12)
Ge(2)–O(5)	1.779(22)	1.759(13)
Ge(2)–O(7)	1.756(22)	1.734(11)
O(1)–R–O(6)	82.3(10)	82.6(7)
O(1)–R–O(2)	75.1(9)	77.9(6)
O(1)–R–O(1′)	67.7(9)	67.3(6)
O(1)–R–O(3)	77.3(9)	76.6(6)
O(1)–R–O(4)	129.2(22)	130.2(15)
O(1)–R–O(4′)	143.5(32)	141.5(21)
O(1)–R–O(7)	141.4(28)	143.7(22)
O(1)–R–O(5)	91.6(11)	90.8(7)
O(1)–R–O(3′)	84.5(9)	82.9(6)
O(1)–R–O(4)	62.8(8)	63.4(5)
O(1)–R–O(4)	117.8(17)	117.0(11)
O(1)–R–O(7)	114.4(15)	116.8(11)
O(1)–R–O(5)	149.1(30)	147.4(19)
O(2)–R–O(1)	74.8(8)	75.8(5)
O(2)–R–O(3)	150.2(30)	151.6(22)
O(2)–R–O(4)	82.0(9)	84.3(6)
O(2)–R–O(4)	141.0(26)	140.3(17)
O(2)–R–O(7)	69.1(8)	69.2(6)
O(2)–R–O(5)	123.4(16)	124.6(10)
O(3)–R–O(4)	107.4(12)	102.8(7)
O(3)–R–O(4)	68.0(8)	66.7(5)
O(3)–R–O(7)	140.3(23)	138.5(16)
O(3)–R–O(5)	68.2(7)	68.2(4)

Table 2. (Continued)

	La	Pr
O(4)–R–O(4)	73.8(8)	71.4(5)
O(4)–R–O(7)	59.6(7)	62.2(5)
O(4)–R–O(5)	138.0(21)	136.1(13)
O(4)–R–O(7)	72.3(8)	71.8(5)
O(4)–R–O(5)	65.8(8)	65.6(5)
O(6)–R–O(2)	64.4(7)	65.1(5)
O(6)–R–O(1)	134.2(21)	134.8(15)
O(6)–R–O(3)	122.6(16)	123.0(10)
O(6)–R–O(4)	126.6(18)	130.1(13)
O(6)–R–O(4)	107.0(13)	107.6(9)
O(6)–R–O(7)	69.8(8)	70.1(6)
O(6)–R–O(5)	59.4(7)	59.7(5)
O(7)–R–O(5)	96.1(10)	95.3(7)
O(3)–Fe–O(4)	98.3(15)	96.0(8)
O(3)–Fe–O(7)	97.1(15)	95.3(8)
O(3)–Fe–O(2)	91.8(13)	95.7(7)
O(4)–Fe–O(7)	89.1(13)	87.5(7)
O(4)–Fe–O(2)	88.6(12)	89.1(6)
O(6)–Fe–O(3)	132.1(27)	132.3(15)
O(6)–Fe–O(4)	129.4(25)	131.6(14)
O(6)–Fe–O(7)	88.9(13)	90.3(7)
O(6)–Fe–O(2)	85.8(12)	84.1(6)
O(7)–Fe–O(2)	171.0(90)	168.8(52)
O(1)–Ge1–O(6)	115.7(23)	114.2(12)
O(1)–Ge1–O(5)	112.4(21)	113.8(12)
O(1)–Ge1–O(4)	101.0(19)	99.4(10)
O(5)–Ge1–O(4)	112.6(20)	112.7(11)
O(6)–Ge1–O(5)	97.6(17)	95.3(9)
O(6)–Ge1–O(4)	118.1(23)	122.3(13)
O(2)–Ge2–O(3)	106.6(18)	106.1(10)
O(5)–Ge2–O(2)	106.7(19)	107.9(11)
O(5)–Ge2–O(3)	109.0(20)	107.2(10)
O(7)–Ge2–O(5)	104.6(18)	103.7(10)
O(7)–Ge2–O(2)	119.5(22)	117.6(11)
O(7)–Ge2–O(3)	110.0(20)	113.9(12)

quickly converged, leading to good discrepancy *R*-factors. The excellent agreement between the observed and calculated neutron profiles of $FePrGe_2O_7$, for example, is shown in figure 1.

The final refined positional and thermal parameters for the neutron analysed La and Pr compounds are given in table 1, and table 2 consists of their main interatomic distances and angles. Table 3 lists the refined lattice parameters, which monotonically decrease from La to Gd as the rare-earth size becomes smaller. A correlation factor of 0.9994 is found between the unit cell volume and r^3, using the Shannon [14] lanthanide ionic radius for nine-coordination with the oxygen.

The structure of the title compounds (figure 2), like that of $GaRGe_2O_7$ [1], contains three coordination polyhedra: chains of flexed RO_9 nanohedra lying along the *a*-axis; Ge(1) and Ge(2) tetrahedra forming Ge_2O_7 diorthogroups along the [001] direction and FeO_5 isolated

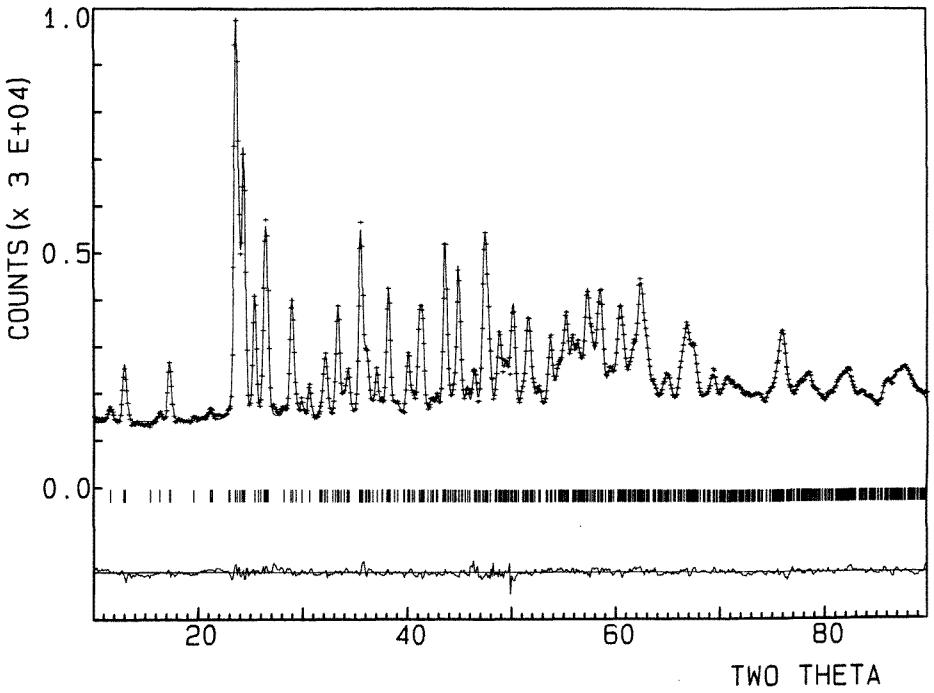

Figure 1. The neutron diffraction profile for $FePrGe_2O_7$ at 295 K. The crosses are the raw data points. The solid line is the best fit profile. The difference plot appears at the bottom. Thick marks indicate the positions of the Bragg $< 90^\circ$ 2θ reflections included in the refinement.

Table 3. Lattice parameters for $FeRGe_2O_7$, R = La, Pr, Nd and Gd. Data and discrepancy factors for R = La and Pr are from NPD refinements.

	La	Pr	Nd	Gd
Lattice parameters				
a (Å)	7.308(1)	7.2422(7)	7.2208(8)	7.141(1)
b (Å)	6.665(2)	6.6361(6)	6.6229(7)	6.5903(7)
c (Å)	13.069(4)	12.986(1)	12.949(1)	12.833(2)
β (°)	117.3(1)	117.13(5)	117.11(5)	117.1(1)
V (Å^3)	566.0(2)	555.44(1)	551.23(7)	537.73(9)
D_c (g cm^{-3})	5.30	5.43	5.51	5.81
No. of reflections	694	679	73	54
Reliability factors				
R_p	3.52	1.99		
R_{wp}	4.77	2.66		
R_{exp}	1.19	1.12		
χ^2	16.1	5.58		
R_I	5.12	3.19		

distorted trigonal bipyramids. The Ge(1)–O(5)–Ge(2) angles (°) are 127.3(23) and 127.7(13) for R = La and Pr, respectively. The Ge(1) tetrahedra share two edges with the rare-earth polyhedra, whereas Ge(2) tetrahedra, more regular than those with Ge(1), share no edges

with other polyhedra. The detailed analysis of the nanohedral arrangement of oxygens around R shows no quadrangular faces, suggesting a tricapped trigonal prism, ttp, as the R coordination polyhedron.

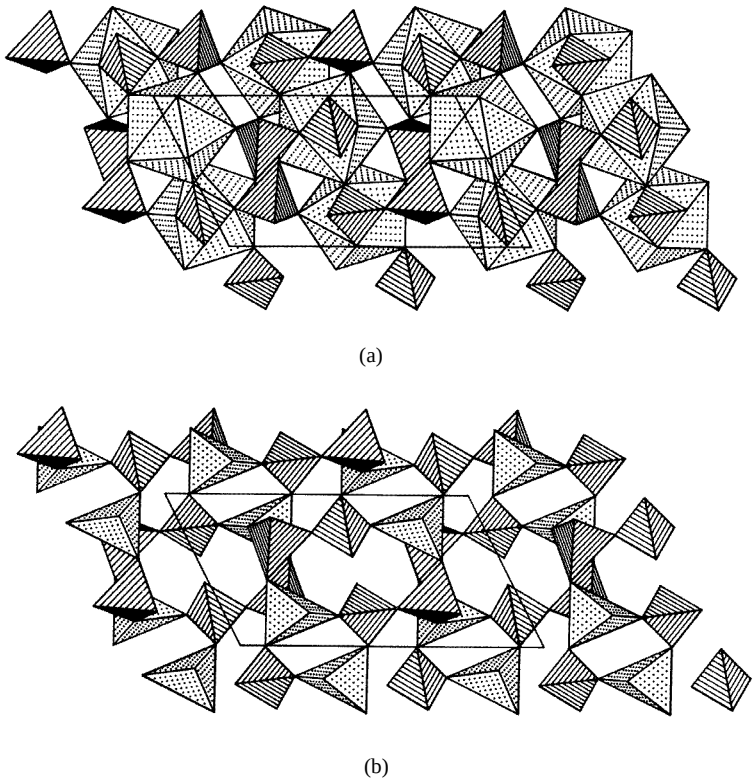

Figure 2. Some a, c-projections of the $FeRGe_2O_7$ structure: (a) chains of RO_9 polyhedra sharing edges with $Ge(1)O_4$ tetrahedra from the Ge_2O_7 groups; (b) FeO_5 trigonal bipyramids linked through each apex to the Ge_2O_7 diorthogroups.

In order to compare some details between $FeLaGe_2O_7$ and $FePrGe_2O_7$, we choose an index, $\Delta d = [\sum(d_m - d_i)^2]^{1/2} \times 10^3$, to define the distortion degree of each polyhedron. Then, although the RO_9 nanohedra are found to be more distorted for R = Pr, the obtained Δd values, 139.5, 109.0 and 41.8 against 116.2, 76.0 and 31.3 for the FeO_5, $Ge(1)O_4$ and $Ge(2)O_4$ polyhedra in $FeLaGe_2O_7$ and $FePrGe_2O_7$ respectively, show the latter compound to be much less distorted than that of La. This is an opposite result to that previously obtained [1] for the isostructural family of Ga and rare-earth germanates, where the decrease in the R size led to more distorted GaO_5, $Ge(1)O_4$ and $Ge(2)O_4$ polyhedra. The average M–O distances in these polyhedra for $FeRGe_2O_7$ (R = La, Pr) agree quite well with the sum of ionic M and O radii [14].

It is interesting to examine the structures of $FeRGe_2O_7$ in the light of the Brown bond valence model [15, 16], which allows the evaluation of stresses in the crystal through the calculation of the valence of the cations and anions present in the solid. This model gives a phenomenological relationship between formal valence and bond length. In perfect nonstrained structures the bond valence sum (BVS) rule states that the formal charge of the cation (anion) is equal to the sum of the bond valences around this cation (anion). This rule

is satisfied only if the stress introduced by the coexistence of different structural units can be relieved by the existence of enough degrees of freedom in the crystallographic structure. The departure from the BVS rule is a measure of the stress existing in the bonds of the structure.

Table 4. Bond valence sums (BVSs) for Fe, R, Ge and O atoms within the respective coordination polyhedra in the $FeRGe_2O_7$ structure R = La and Pr. Bond valences are calculated for each individual bond as $s_i = \exp[(r_0 - r_i)/B]$; $B = 0.37$; r_0(La) = 2.172, r_0(Pr) = 2.135, r_0(Fe) = 1.759 and r_0(Ge) = 1.748 Å for the R^{III}–O^{2-}, Fe^{III}–O^{2-} and Ge^{IV}–O^{2-} pairs, respectively (from [16]) Individual La–O and Ni–O distances are taken from table 2. Bond valence sums are obtained as BVS = Σs_i.

	La	Pr
Fe	3.07	3.01
R	3.02	3.12
Ge(1)	4.21	4.12
Ge(2)	3.78	3.88
O(1)	2.09	2.08
O(2)	1.68	1.81
O(3)	1.93	1.92
O(4)	1.84	2.02
O(5)	2.11	2.15
O(6)	2.31	2.32
O(7)	1.87	1.83

Table 4 lists the valences calculated for La(Pr), Fe, Ge and O from the individual La(Pr)–O, Fe–O and Ge–O distances of table 2. In the Pr compound, a moderate deviation of the calculated valences of Pr, Ge(1) and Ge(2) from the expected values of +3, +4 and +4, respectively, can be observed. According to that, Pr and Ge(1) are slightly overbonded, while Ge(2) is correspondingly underbonded. This trend is still more patent in the La germanate, in which Ge(1)/Ge(2) exhibit valences remarkably higher/lower than +4, giving rise to increasing structural stresses in the crystal, and the metastable character of the structure.

The structural stability can be quantified in some extent by means of the calculation of the so-called 'global inestability index' (GII), which is obtained as the root mean square of the existing BVS deviation for all the N atoms present in the asymmetric unit, $GII = \sqrt{(\sum[BVS_i - V_i]^2/N)}$. GII is a measure of the extent to which the BVS rule is violated over the whole structure [17]. For La and Pr germanates, we obtain GII values of 0.18 and 0.15 valence units (v.u.) respectively, which suggests a lower stability for the La structure. In fact, the GII values are both close to 0.2 v.u., which already indicates the presence of intrinsic strains large enough to cause instability at room temperature, as suggested by Brown [17] and Armbruster *et al* [18]. Moreover, the Fe–R–Ge–O presents an alternative form [6] for the smaller rare-earth cations, which is probably able to relax the relatively high stress observed here.

The characteristic IR absorptions for $FeRGe_2O_7$ (R = La, Pr, Nd, Gd) are shown in figure 3. Comparing the general structure of these band-rich spectra it can be seen that they are very similar if not totally identical over the whole frequency range. The positions of the measured spectral bands are given in table 5. Although it is not possible to make even an approximate assignment, some tentative attributions, especially for the $Ge_2O_7^{6-}$ groups, can be proposed according to the available literature [19, 20]. In effect, it is clear that the high-frequency observed bands correspond to the pyrogermanate groups, whose

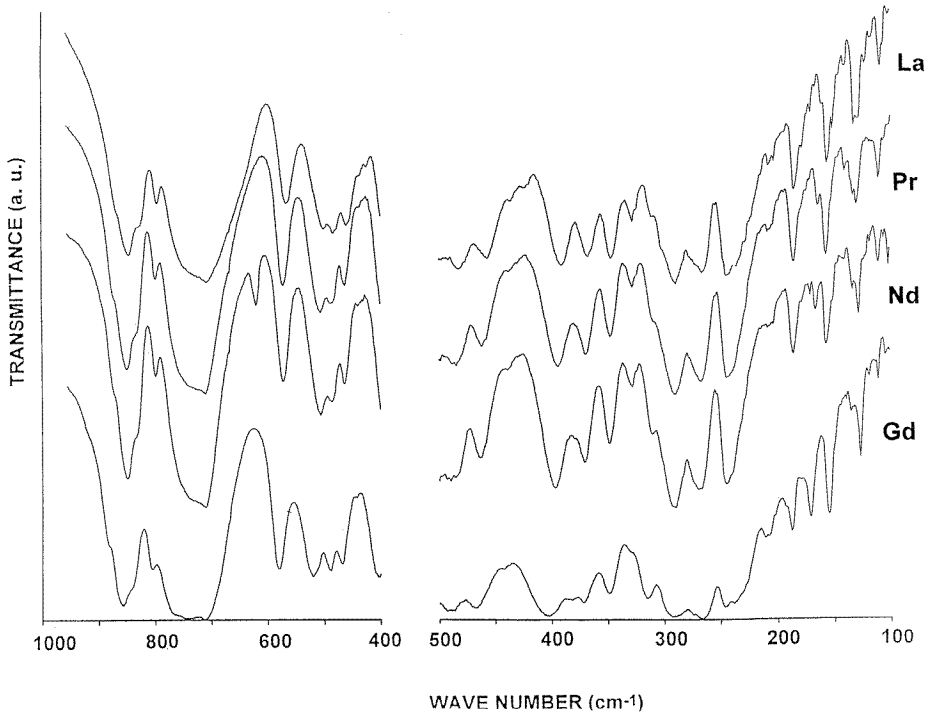

Figure 3. IR spectra for $FeRGe_2O_7$ R = La, Pr, Nd and Gd.

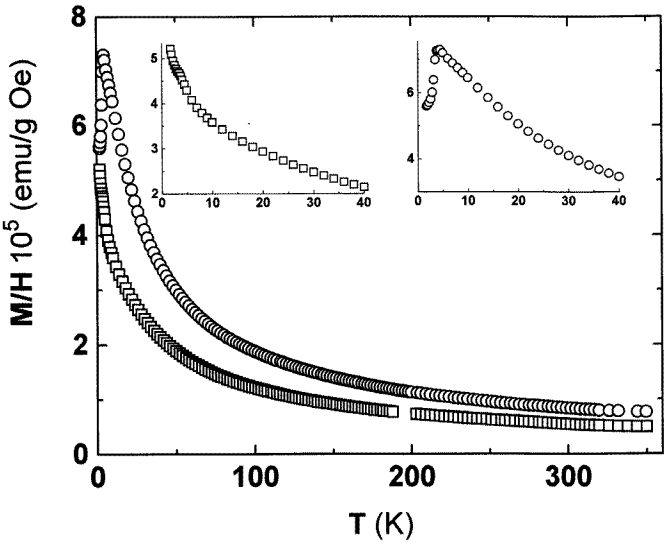

Figure 4. dc magnetic susceptibility against T for $FeRGe_2O_7$ (R = La (□); Pr (○)).

normal vibrations are classified into in-phase and out-of-phase coupling motions of terminal GeO_3 group vibrations and the skeletal vibrations of the Ge–O–Ge bridge. The comparison

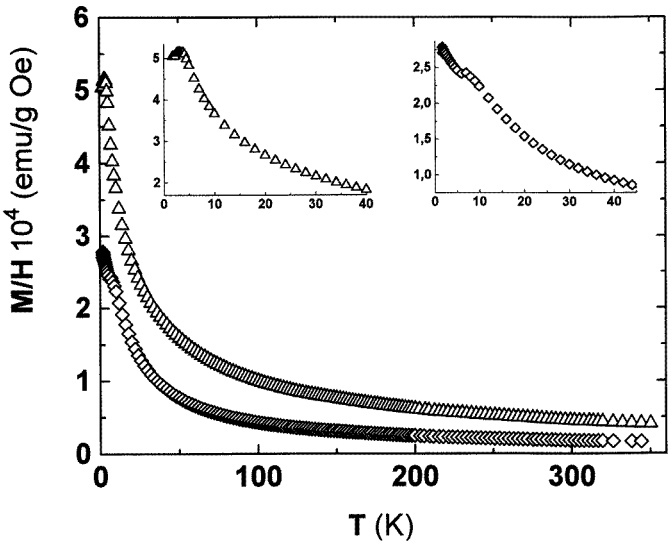

Figure 5. dc magnetic susceptibility against T for $FeRGe_2O_7$ (R = Nd (△); Gd (◊)).

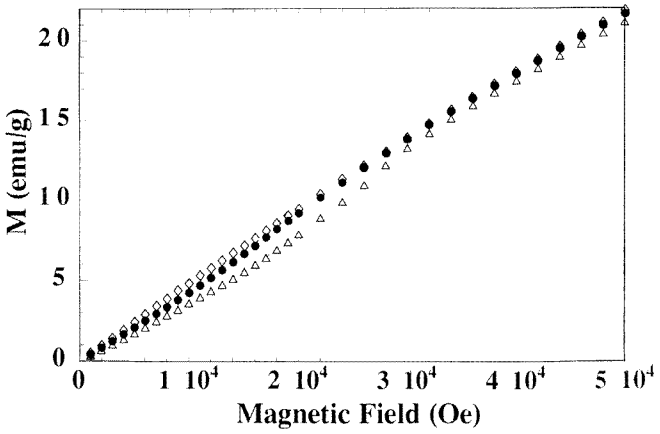

Figure 6. Magnetization isotherms for $FePrGe_2O_7$: (△), 1.8 K; ● , 3 K; ◊, 4 K.

with the assignments made on linear-bridge pyrogermanates [20] of the type $A_2Pb_2Ge_2O_7$ (A = K, Rb, Cs) strongly supports the attribution of the highest IR band, near 850 cm^{-1}, to the antisymmetric stretch ν_a of the Ge–O–Ge bridge. According to some studies [19] and for bridging angles larger than 115°, ν_a is at least 215 cm^{-1} higher than the symmetric bridge stretching, ν_s, and the separation increases as the bridge angle increases, being these separations of $\sim$ 400 cm^{-1} in the above-mentioned linear pyrogermanates [20]. Thus, it will be the band at 566–580 cm^{-1} (from La to Gd compounds), that could be assigned to ν_s of the bridge. Following the same vibrational description, the remaining high-frequency bands observed, first near 800 cm^{-1} and then ranging between $\sim$ 710 and 770 cm^{-1}, can be assigned to the various stretching vibrations of the GeO_3 terminal groups; and the bending modes from either the GeO_3 or the bridge would correspond to some absorption peaks lying

Table 5. Band positions (cm^{-1}) of the infrared spectra of RFeGe$_2$O$_7$ (R = La, Pr, Nd, Gd). s, strong; m, medium; w, weak; vw, very weak; sh, shoulder; vbr, very broad.

$LaFeGe_2O_7$	$PrFeGe_2O_7$	$NdFeGe_2O_7$	$GdFeGe_2O_7$
866.9 sh	872.7 sh	871.8 sh	880 sh
845.3 s	849.2 s	849.2 s	857.1 s
827.7sh	831.6 sh	835.5 sh	841.4 sh
795.4 m	798.3 m	798.3 m	806.2 m
—	—	—	769.0 s
—	—	741.6 s	745.5 s
708.3 s, vbr	710.2 s, vbr	710.2 s, vbr	713.2 s, vbr
668.1 sh	667.2 sh	669.1 sh	687.7 sh
566.3 m	572.2 m	572.2 m	580.0 m
499.8 s	505.6 s	505.6 m	520.3 s
483.1 s	487.0 s	484.1 m	489.0 s
459.6 s	462.6 s	462.6 m	467.5 s
437.0 vw	438.5 vw	439.5 vw	442.9 vw
425.2 vw	—	—	—
390.7 m	394.7 m	397.1 m	402.0 m
—	—	—	381.9 vw
367.6 m	370.0 m	370.5 m	372.0 m
346.9 m	347.9 m	348.9 m	349.2 m
328.2 w	328.2 w	328.2 vw	331.2 vw
325.3 sh	324.8 sh	324.3 sh	—
311.0 sh	309.0 w	311.0 m	314.9 m
302.6 sh	—	—	—
289.3 m	289.8 m	292.3 m	292.8 m
266.2 m	267.7 m	267.9 m	265.7 m
245.0 m	244.5 m	245.0 m	246.5 m
236.2 sh	—	240.1 sh	238.6 m
214.5 vw	215.0 sh	214.0 vw	
208.1 vw	208.6 vw	208.4 vw	209.1vw
185.0 m	185.0 m	185.5 m	185.5 m
177.6 sh	—	—	—
170.7 sh	—	—	170.7 m
161.3 sh	162.8 vw	165.3 w	—
155.9 m	155.9 m	156.4 m	154.9 m
151.5 sh	151.5 sh	150.5 sh	—
132.3 w	131.8 vw	132.8 vw	131.8 vw
128.8 w	128.4 w	127.4 w	125.9 w
108.7 w	109.2 w	109.6 w	110.1 vw

below 500 cm^{-1}. In the same range, below 500 cm^{-1}, many other possible contributions must be taken into account, not only those from the lanthanide–oxygen bond stretching [21], but also from the FeO_5 polyhedra stretching. The low-frequency absorption peaks, below $\sim$ 300 cm^{-1}, may be due to the remaining bending vibrations of the different coordination polyhedra present in the structure. In any case, despite the complexity of the spectra, the expected slight band displacement to higher frequencies, which parallels the diminution of unit-cell dimensions from R = La to R = Gd can be observed here with certainty. This behaviour, often observed in isostructural lanthanide compounds [22], is usually related to a reinforcement of the metal–oxygen bonds associated to the contraction of the cell volumes.

The temperature dependence of the $FeRGe_2O_7$ magnetic susceptibility χ is shown in figures 4 and 5 for R = La and Pr, and Nd and Gd, respectively. If the magnetic

behaviour of $FeLaGe_2O_7$, which has only Fe^{3+} as paramagnetic ion, is first considered, a slight curvature in the χ^{-1}–T plot is observed, with a magnetic moment becoming smaller when the temperature decreases, then, in contradiction with previously reported results [7], a Curie–Weiss law is not followed in the observed temperature range between 1.7 and 350 K. No indication of antiferromagnetic ordering in the Fe^{3+} sublattice was found. The observed inflection point at very low temperatures may be due to some paramagnetic impurities. Very clear maxima are observed, however, for $FePrGe_2O_7$ and $FeNdGe_2O_7$ at 4.3 K and 3.5 K respectively, and below these temperatures the susceptibilities sharply decrease, confirming [7] the existence of an antiferromagnetic ordering in the rare-earth sublattice. Under the same conditions, $FeGdGe_2O_7$ shows below 15 K upward deviations from linearity in the χ^{-1}–T plot, and an inflection point at 5.8 K which would be an indication of the antiferromagnetic ordering of the Gd^{3+} cations. The antiferromagnetic ordering in the rare-earth sublattice would be gradually induced by the polarization of Fe^{3+}, in the same way that was found and explained [23–25] for Co^{2+} and Cu^{2+} ions in the phases R_2BaMO_5, and could justify the observed reduction of the magnetic moment.

Magnetization curves in magnetic fields up to 50 kOe show that, at $T \leqslant 10$ K, the magnetization varies linearly with the field, except for $FePrGe_2O_7$ (figure 6), for which a very weak increase at 1.8 K in a field of ~ 22 kOe can be observed.

Neutron diffraction measurements are now in progress in order to establish the magnetic structures of these oxides.

Acknowledgments

This work was supported by the CICYT of Spain, under project No PB94-0031. We thank Dr J L Martínez for performing the magnetic measurements. One of the authors (LB) acknowledges a fellowship from the Consejo Nacional de Ciencia y Tecnología (CONACYT), Mexico.

References

[1] Kaminskii A A, Mill B V, Butashin A V, Belokoneva E L and Kurbanov K 1987 *Phys. Status Solidi* a **103** 575
[2] Campá J A, Cascales C, Gutiérrez-Puebla E, Mira J, Monge M A, Rasines I, Rivas J and Ruíz-Valero C 1995 *J. Alloys Compounds* **225** 225
[3] Campá J A, Cascales C, Gutiérrez-Puebla E, Monge M A, Rasines I and Ruíz Valero C 1995 *J. Solid State Chem.* **120** 254
[4] Campá J A, Gutiérrez-Puebla E, Monge M A, Ruíz-Valero C, Mira J, Rivas, Cascales C and Ruíz-Valero C *J. Solid State Chem.* at press
[5] Jarchow J, Klaska K H and Schenk-Strauss H 1985 *Z. Kristallogr.* **172** 159
[6] Kazei Z A, Kuyanov I A, Levitin R Z, Markosyan A S, Mill B V, Reiman S I, Snegirev V V and Tamazyan S A 1989 *Sov. Phys.–Solid State* **31** 233
[7] Mill B V, Kazei S A, Reiman S I, Tamazyan S A, Khamdamov F D and Bykova L Yu 1987 *Vestn. Mosk. Gos. Univ. Fiz. Astron.* **28** 95
[8] Appelman D E and Evans H T 1973 *Indexing and Least-squares Refinement of Powder Diffraction Data* (Washington, DC: US Geological Survey)
[9] Rietveld H H 1969 *J. Appl. Crystallogr.* **2** 65
[10] Rodríguez-Carvajal R 1990 *Abstracts Satellite Meeting XVth Congr. Int. Union Crystallogr. (Toulouse, 1990)* p 127
[11] Wiles D B and Young R A 1982 *J. Appl. Crystallogr.* **15** 430
[12] Yvon R, Jeitschko W and Parthé E 1977 *J. Appl. Crystallogr.* **10** 73
[13] Boudreaux E A and Mulay L N 1976 *Theory and Applications of Molecular Paramagnetism* (New York: Wiley) pp 494–5

[14] Shannon R D 1976 *Acta Crystallogr.* A **32** 751
[15] Brown I D 1981 *Structure and Bonding in Crystals* vol 2, ed M O'Keefe and A Navrotsky (New York: Academic) pp 1–30
[16] Brese N E and O'Keefe M 1991 *Acta Crystallogr.* B **47** 192
[17] Brown I D 1992 *Z. Kristallogr.* **199** 255
[18] Armbuster T, Röthlisberger F and Seifert F 1990 *Am. Mineral.* **75** 847
[19] Nakamoto K 1986 *Infrared and Raman Spectra of Inorganic and Coordination Compounds* 4th edn (New York: Wiley) pp 165–6
[20] Tarte P, Pottier M J, Procès A M 1973 *Spectrochim. Acta* A **29** 1017
[21] Baran E J, Vassallo M B and Cascales C 1994 *An. Asoc. Quim. Argent.* **82** 215
[22] Botto I L, Baran E J, Cascales C, Rasines I and Sáez-Puche R 1991 *J. Phys. Chem. Solids* **52** 431
[23] Hernandez Velasco J 1992. *MsD Thesis* Universidad Complutense de Madrid
[24] Salinas Sánchez A J 1992 *PhD Thesis* Universidad Complutense de Madrid
[25] Salinas Sánchez A, Sáez-Puche R and Alario Franco M A 1990 *J. Solid State Chem.* **89** 361